Published in final edited form as:
Semin Musculoskelet Radiol. 2008 September ; 12(3): . doi:10.1055/s-0028-1083109.

Novel Contrast Mechanisms at 3 Tesla and 7 Tesla

Ravinder R. Regatte, Ph.D.[1] and **Mark E. Schweitzer, M.D.**[1]
[1]Center for Biomedical Imaging, Department of Radiology, New York University School of Medicine, New York, New York

Abstract

Osteoarthritis (OA) is the most common musculoskeletal degenerative disease, affecting millions of people. Although OA has been considered primarily a cartilage disorder associated with focal cartilage degeneration, it is accompanied by well-known changes in subchondral and trabecular bone, including sclerosis and osteophyte formation. The exact cause of OA initiation and progression remains under debate, but OA typically first affects weightbearing joints such as the knee. Magnetic resonance imaging (MRI) has been recognized as a potential tool for quantitative assessment of cartilage abnormalities due to its excellent soft tissue contrast. Over the last two decades, several new MR biochemical imaging methods have been developed to characterize the disease process and possibly predict the progression of knee OA. These new MR biochemical methods play an important role not only for diagnosis of disease at an early stage, but also for their potential use in monitoring outcome of various drug therapies (success or failure). Recent advances in multicoil radiofrequency technology and high field systems (3 T and above) significantly improve the sensitivity and specificity of imaging studies for the diagnosis of musculoskeletal disorders. The current state-of-the-art MR imaging methods are briefly reviewed for the quantitative biochemical and functional imaging assessment of musculoskeletal systems.

Keywords

Osteoarthritis; T2; dGEMRIC; $T1_\rho$; sodium MR; CEST

OSTEOARTHRITIS

Osteoarthritis (OA) is one of the most common forms of musculoskeletal disease. It affects millions of Americans, particularly the elderly population.[1–5] The economic burden of OA is expected to increase substantially over the next decade due to the growing aging population and the increasing prevalence of obesity. The clinical symptoms of OA are pain, stiffness, and functional impairment, and current treatment options are focused mostly on symptomatic relief rather than modifying the OA disease process.

The pathophysiology of OA is incompletely understood. The principal pathological hallmark of OA is slowly developing, degenerative breakdown of articular cartilage with associated changes in subchondral bone, bone marrow, and synovium. OA may be aggravated by numerous risk factors, including joint malalignment, obesity, trauma, meniscal abnormalities, cruciate ligament tears, biochemical, biomechanical, genetic, and environmental factors, and surgical interventions.[6–9]

Address for correspondence and reprint requests: Ravinder R. Regatte, Ph.D., NYU-Hospital for Joint Diseases, Department of Radiology, 301 East 17th St., New York, NY 10003 (ravinder.regatte@med.nyu.edu).

Conventional radiographs are the current imaging gold standard used to diagnose OA and monitor disease progression in clinical trials. Often used for this is the Kellgren-Lawrence grading system based on joint space width and osteophyte scores, but radiographs are limited for early disease due to the inability to detect early chondral abnormalities, the inability to measure cartilage loss directly, and the use of ionizing radiation.[10–15] Several advanced medical imaging methods are currently available to assess disease status.[16–73] Although arthroscopy is the gold standard for early detection of chondral defects, it has several limitations, such as the invasiveness of the procedure and the subjectivity of technique and interpretation.

Three-dimensional (3D) magnetic resonance (MR) imaging is well suited for noninvasive, nondestructive, multiplanar visualization of the whole knee joint due to its excellent soft tissue contrast.[74–76] MR imaging of humans at very high magnetic fields (≥3 T) has potential benefits in terms of increased signal-to-noise ratio (SNR)/spatial resolution, higher susceptibility contrast, improved sensitivity for low gamma nuclei, and larger spectral dispersion for spectroscopy applications. High field (≥3 T) systems have seen rapidly increasing use for exploring potential musculoskeletal applications due to their high intrinsic SNR, potential higher resolution (spatial, temporal), and improved contrast.

This article focuses specifically on high field applications of musculoskeletal systems in general and articular cartilage in particular. Most musculoskeletal tissues (cartilage, muscle, menisci, bone, tendon, ligaments, etc.) at standard clinical scanners (1.5 T) exhibit low SNR, which can be exacerbated by the small field of view necessary. For high field systems (≥3 T), particularly at 7 T, there are several challenges for musculoskeletal imaging, such as homogeneous radiofrequency (RF) coil design, increased chemical shift artifacts, susceptibility artifacts, RF energy deposition, as well as change in relaxations times when compared with more typical 1.5-T clinical scanners. Despite these issues, MRI at high field systems likely will provide excellent opportunities for quantitative high-resolution morphological, biochemical (molecular), and functional imaging of musculoskeletal systems. In this article, the current state-of-the-art high field imaging techniques (morphometry, delayed gadolinium-enhanced MRI of cartilage [dGEMRIC], T2, diffusion, $T1_{\rho}$, sodium MRI, chemical exchange dependent saturation transfer [CEST]) for quantitative biochemical and functional imaging assessment of musculoskeletal systems are reviewed.

ARTICULAR CARTILAGE COMPOSITION AND STRUCTURE

Articular cartilage is a connective tissue primarily consisting of extracellular matrix (ECM) with a relatively small fraction of cells called chondrocytes. The major components of the ECM are proteoglycans (~3 to 10%), type II collagen (~15 to 20%), water (~65 to 80%), and small amounts of noncollagenous proteins.[77–80]

Biomechanically cartilage has remarkable viscoelastic properties and acts like a shock absorber with a low coefficient of friction. Proteoglycans (PGs) are highly charged macromolecules with a central core protein to which glycosaminoglycans (GAGs) are attached. The three major side chains in cartilage are chondroitin 4-sulfate (CS-4), chondroitin 6-sulfate (CS-6), and keratin sulfate (KS).[81–83] The chondroitin sulfates are the major subunits in cartilage and account for 55 to 90% of total GAGs. The GAGs have a concentration of negatively charged sulfate groups that attract positive ions and water molecules to maintain electroneutrality. The strong water-binding affinity of PGs produces an osmotic pressure that must be counterbalanced by restraining forces in the collagen fibrils network. These collagen fibrils form a highly organized anisotropic fibrous network that leads to the extremely high tensile and shear strength of cartilage. The main amino acid residues of collagen are glycine, alanine, proline, hydroxyproline, and hydroxylysine[41,78].

PGs provide much of the compressive stiffness of cartilage through electrostatic repulsion.[84] Collagen fibers in cartilage are generally weakly hydrated, highly structured, and depth dependent.

Articular cartilage is subdivided into three histological zones based on the collagen structural orientation. The collagen fibrils are densely packed and orientated parallel to the articular surface in the superficial zone, randomly oriented in the transitional zone, and perpendicular to the articular surface in the radial zone. The deepest region of the cartilage is the calcified region, which separates the articular cartilage from the subchondral bone. The characteristic regular arrangement of collagen fibers in articular cartilage not only leads to the magic-angle effect but also demonstrates magnetization transfer and diffusion anisotropic phenomenon on specific MR sequences.[57,59–61,85–88]

Currently Available Magnetic Resonance Imaging Methods for Osteoarthritis

The most common mechanisms of MR contrast are T1, T2, and proton density. These MR contrast mechanisms may be manipulated by adjusting several imaging parameters (repetition time, echo time, flip angle, etc.). The intrinsic tissue relaxation parameters are the major determinants of image contrast between musculoskeletal tissues such as cartilage, synovial fluid, bone marrow, skeletal muscle, ligaments, tendons, and so on. The specific type of imaging sequence (T1 or T2 weighted) can be used to improve the contrast between pathological lesions and surrounding tissues. In some cases, the specificity of diagnosing cartilage lesions can be improved by suppressing fat or synovial fluid. T1 and T2 relaxation parameters vary with static magnet field strength.[25,31] As a result, these imaging parameters have to be specifically adjusted to obtain similar contrast at different static field strengths (for example, 1.5 T versus 3.0 T or 3 T versus 7 T).

Several imaging methods have been developed to assess OA disease status quantitatively as well as monitor disease progression in longitudinal investigations. For example, recent ongoing multicenter studies as part of the Osteoarthritis Initiative (OAI) funded by the National Institutes of Health (http://www.niams.nih.gov/ne/oi) have started acquiring longitudinal data on >4000 human subjects. These studies aim specifically to identify sensitive imaging biomarkers to diagnose and distinguish symptomatic knee OA progression versus incidental OA. These MR imaging methods are broadly divided into two types: cartilage morphometry (CM) and biochemical imaging methods.

CARTILAGE MORPHOMETRY

CM studies have focused on quantifying the overall or more focal anatomical alterations, which includes cartilage volume, mean cartilage thickness, and mean cartilage surface area.[35,89–94] High-resolution 3D T1-weighted (sagittal or coronal) fast low-angle shot (FLASH) with fat suppression (or water excitation) or fast double echo and steady state (DESS) with water excitation imaging sequences have been used to acquire data due to optimized contrast between cartilage, synovial fluid, and surrounding tissues.[40,95] The DESS has higher T2 weighting resulting in bright cartilage signal intensity and synovial fluid; FLASH has preferential T1 weighting (improves contrast between cartilage and synovial fluid). Recently Eckstein et al[40,95] compared the test-retest precision (pilot OAI study) of a DESS imaging sequence with water excitation with that of previously validated FLASH sequence with water excitation. Manual as well as semiautomatic segmentation methods have been used to segment the cartilage in each compartment.

Conflicting morphometry results have been reported, especially in cross-sectional studies due to the number of covariables, including joint size, bone size, age, sex (e.g., women have smaller joint surfaces than men), heterogeneity of the disease, cartilage swelling in early

OA, diurnal variation in cartilage, daily physical activity of the person, and so on.[96–98] Consequently, some research groups have suggested that the cartilage volume is an insensitive imaging marker for disease progression; other studies found that cartilage volume can predict the disease progression. Longitudinal studies have shown some promising results, especially in regional compartment alterations in cartilage thickness over a specific period of time.[40] Cartilage morphometry (Fig. 1) studies dealing with measurement of cartilage thickness, volume, surface area, and their advantages and drawbacks are elegantly described in review articles.[32,35,36,65,66,99–101]

BIOCHEMICAL IMAGING METHODS

In addition to cartilage morphometry, the ability to measure and quantify early stage biochemical and structural changes are increasingly important for OA disease management and therapy. The use of early biochemical and structural imaging techniques have been rapidly growing in recent years due to the development of high field systems (≥3 T) and multi-coil technology (phased array coils) with parallel imaging capability. Based on the different macromolecules in cartilage, several different imaging strategies were developed to quantify the biochemical imaging markers.

The early biochemical changes in OA include loss of macromolecules (predominantly GAG) with minor structural changes (collagen) and increased water content. These different biochemical and structural imaging biomarkers can be quantified via dGEMRIC, transverse relaxation time constant (T2), spin-lattice relaxation time in the rotating frame ($T1_\rho$), sodium (^{23}Na) MRI, magnetization transfer (MT) contrast, diffusion imaging, and CEST approaches. Some of the biochemical imaging techniques requires either exogenous contrast agents (e.g., dGEMRIC) or RF hardware modifications with specialized RF coils (e.g., ^{23}Na MRI).

Delayed Gadolinium-Enhanced Magnetic Resonance Imaging of Cartilage

Gadolinium (Gd)-enhanced imaging can indirectly assess and quantify the GAG concentration in cartilage. Diethylenetriamine penta-acetate [$Gd(DTPA)^{2-}$], being anionic, distributes in cartilage inversely to the concentration of negatively charged GAGs due to charge repulsion. The distribution of $Gd(DTPA)^{2-}$ in the knee joint can be determined from MR measurements of T1 mapping 90 minutes following intravenous contrast agent injection (0.2 mM/kg). This protocol also requires 10 minutes of joint exercise for effective diffusion of contrast agent into the cartilage. Recently it has been reported that the contrast agent dose should be adjusted for body mass index rather than weight of the subject[102] to account for variability in biodistribution of Gd(DTPA).[2] Although most of the initial dGEMRIC studies have been limited to either single-slice or multi-slice two-dimensional (2D) methods (inversion-recovery prepared fast spin echo), more recently several investigators[16,17,51,52,67,103,104] have demonstrated and validated the in vivo feasibility of 3D methods inversion-recovery (IR) FLASH, Look Locker scheme, IR-true-FISP (fast imaging with steady-state precession), and variable flip angle method with parallel imaging for quantitative assessment of GAG in cartilage (Fig. 2). dGEMRIC has potential clinical applications for identification of early biochemical changes in knee and hip OA patients. However, recently it has been shown in patients with kidney impairment[105,106] that the use of Gd-based contrast agents may trigger a rare but severe medical complication known as nephrogenic systemic fibrosis or nephrogenic fibrosing dermopathy. In light of these reports, the U.S. Food and Drug Administration (FDA) has issued a public health advisory to limit use of Gd-based contrast agents based on a patient's risk/ benefit ratio (http://www.fda.gov/cder/drug/advisory/gadolinium_agents.htm). More likely this technique will remain limited to research studies secondary to its time requirements, expense, and risk.

Cartilage T2 Mapping

T2 relaxation mapping is a noninvasive imaging method for evaluating the structural integrity of various biological tissues. T2 mapping is a sensitive tool for probing slow molecular interactions in cartilage. The quantitative assessment of cartilage T2 mapping has potential for evaluating and monitoring the structural changes in collagen and water content.[18,33,34,62,107–117] Spatial T2 maps are generated from a series of multiecho spin-echo images by fitting the signal intensity of each pixel to a mono-exponential decay. Some groups are using spiral T2 mapping sequences.[31,118]

The acquisition times of T_2 mapping generally range from 10 to 20 minutes depending on the spatial resolution, static field strength, and imaging parameters. Spatial distribution of the cartilage T2 mapping may provide areas of focal chondral defects either due to ultrastructural changes in collagen or increasing/decreasing water content. Most of the prior studies have found negligible effect on T2 mapping following PG depletion of cartilage. However, there was a strong inverse correlation between cartilage T2 mapping and collagen fiber anisotropy measured by polarized light microscopy.[110,112,119] Sensitivity to ultrastructural changes in the collagen matrix, orientation dependence, and changes in water content make the T2 mapping method a useful probe for assessing OA progression.[18,22,114,117,120] Several investigations have demonstrated a strong correlation between T2 and histology in cartilage tissue specimens.[59,61,62,110,112] Elevated T2 relaxation times were reported in OA patients as well as in-vitro tissue specimens by several investigators.[18,22,114,117,120] Xia et al[60] studied extensively the angular dependence of T2 of ex vivo cartilage specimens with respect to static magnetic field using high-resolution microscopy (~14 um). Mosher et al[18,88,117] demonstrated the age, physical exercise, and depth-dependent spatial variations in T2 of cartilage, initially near the articular surface and progressing to deeper regions with increasing age. Fig. 3 shows representative T2 maps obtained from an OA subject. One of the advantages of the T2 mapping sequence is that it does not require any exogenous contrast agent or special hardware or RF coils and is available on almost all standard clinical scanners. It is, however, limited in that the signal changes come predominantly from collagen alterations, which represent somewhat later alterations in the degenerative cascade.

Diffusion Imaging

Diffusion-weighted imaging (DWI) is a useful technique for cartilage imaging that can provide direct visualization of the 3D architecture of cartilage and provide directional information about collagen fibers and their integrity. The mobility of water through macromolecules is important because cartilage is an avascular tissue. It has been reported that the apparent diffusion coefficient (ADC) increases with micromolecular depletion (proteoglycan and collagen).[121–124] To compute an ADC map, a series of images is acquired with different applied diffusion gradients (b-value). The DWI signal intensity is directly proportional to the diffusivity. The diffusion gradients induce a net phase change for moving spins depending on the distance they have moved, resulting in signal loss.

An extended application of ADC mapping is diffusion tensor (i.e., fractional anisotropy) mapping, which gives an estimate of diffusion anisotropy that could be related to cartilage matrix damage.[122,124] However, in vivo diffusion measurements of cartilage are a major challenge in the field of cartilage imaging, especially due to the short T2 relaxation time of cartilage and smaller thickness of the cartilage. The T2 relaxation time of cartilage varies between 10 and 50 ms, necessitating a short echo time (TE) to maximize the cartilage signal. Applying diffusion-sensitizing gradients, however, allows increased TE but renders the sequence sensitive to motion. Therefore, motion correction is often required before accurate

reconstruction can be done. Single-shot diffusion techniques may be implemented, but they have limited SNR and resolution and are likely limited to ≥3 T.

$T1_\rho$ Mapping

$T1_\rho$ is a magnetic relaxation time constant that was described as early as 1955[125] but only recently has been applied to several organs. $T1_\rho$ provides improved contrast between normal and pathological lesions based on the intrinsic biophysical properties of tissues when compared with conventional T1- and T2-weighted imaging. In fact, the value for $T1_\rho$ is always between T2 and T1. T1 and T2 relaxation times are intrinsic properties of tissue and are virtually never affected by pulse sequence parameters. Conventional T1 and T2s are affected by the main magnetic field. However, $T1_\rho$ is unique in that its value is determined by both properties of tissues as well as features of the applied spin-locking pulse. By changing the amplitude of the spin-locking pulse, we can alter the spin-locking frequency and therefore improve the contrast between normal and pathological lesions. The dependence of $T1_\rho$ on the amplitude of the applied spin-locking field is known as $T1_\rho$ dispersion.

$T1_\rho$ dispersion is also a property of the tissue, which can reflect the protein content and composition of tissue[126,127]. In $T1_\rho$ MRI, the magnetization was prepared with a spin-lock pulse cluster that consists of three RF pulses. It starts with a 90-degree hard pulse followed by a long spin-lock pulse of lower power with a phase of 90 degree relative to the first pulse. The length of the spin-lock pulse is denoted as time of spin lock (TSL). During the spin-lock pulse, the transverse magnetization of the spins undergoes relaxation with the rate $1/T1_\rho$. The spin-lock RF pulse cluster ends with a 90-degree hard pulse whose phase is shifted 180 degrees relative to the first 90-degree hard pulse. This pulse takes the transverse magnetization back to the longitudinal axis before any imaging sequence. Here we used a composite spin-lock pulse (self-compensating) that consists of two pulses of equal length (TSL/2) and opposite phase (90 degrees and 270 degrees) to minimize the effects of B_1 field inhomogeneities.[26,27,49]

$T1_\rho$ relaxation time has been proposed recently as both a sensitive and specific marker for early OA.[20,128,129] This method probes spin-interaction processes occurring at low frequencies (100 Hz to 100 kHz). Several investigators have applied the 2D-$T1_\rho$-weighted imaging to various pathologies such as tumor models, brain, muscle, and myocardium in general and connective tissues in particular (articular cartilage and intervertebral disk), employing standard 1.5-T clinical as well as higher field research scanners.[21–24,26,27] Recently, rapid 3D in vivo $T1_\rho$ mapping techniques of knee cartilage at high fields (3 T) have been developed[22,23,26,27] and applied to asymptomatic as well as patients with OA (Fig. 4).

The major advantage of the $T1_\rho$ mapping sequence, similar to T2 mapping, is that it does not require any exogenous contrast agent or special hardware or RF coils. However, the imaging sequence is not currently available on all standard clinical scanners, and it deposits a significant amount of RF energy in tissues.

Sodium Magnetic Resonance Imaging

Sodium plays an important role in cellular function, synaptic transmission, osmotic balance, and solute transport in biological tissues.[130–134] The ^{23}Na nucleus is the only naturally occurring nucleus of sodium with a quantum spin number (I) 3/2. This implies there are four possible orientations of the sodium nucleus with respect to the static external magnetic field (B_0). These four quantum states are characterized by the magnetic quantum number (m), with “m” taking values of +3/2, +1/2, −1/2, and −3/2 for the four quantum states. Sodium

MRI is one of the reference standard methods for measuring GAG in cartilage via single-quantum and multiple-quantum filtered imaging.[135,136] Although ^{23}Na is the most abundant in nature (~100%), it has a low gyromagnetic ratio (11.3 MHz/T) when compared with conventional proton (42.6 MHz/T).

In general, the sensitivity of the nucleus is directly proportional to $\gamma^{11/4}$ I(I +1) for a given B_0 field. For example, the Larmor frequency of sodium and hydrogen at 3 T is 33.8 MHz and 126 MHz, respectively. Average in vivo sodium concentrations are in the range of 250 mM to 350 mM in connective tissues (articular cartilage, intervertebral disk). The MR sensitivity for ^{23}Na is only 9.2% of the 1H MR and the in vivo concentration is ~366 times lower than the in vivo water proton concentration. The combination of these factors results in a ^{23}Na signal that is ~3963 (2.52×10^{-4}) times smaller than the ^{1}H signal.

The MR relaxation properties of a nucleus depend on its neighboring environment and its interactions that perturb the dominant Zeeman field in a significant manner. The most important interaction experienced by sodium nuclei is that between the nonspherically symmetrical nucleus and surrounding electric field gradients. This is called the quadripolar interaction. The magnitude of the quadripolar interaction is determined by the mean square field gradient created by distribution of the fluctuating charge surrounding the sodium nucleus. Sodium nuclei are also involved in chemical exchange resulting from the movement of spins from one chemical environment to another. In general, sodium in solids/liquid crystals experience most of these interactions, whereas in liquids, the static quadripolar interaction is averaged to zero. In the intermediate regimes such as biological systems, the quadripolar interaction is incompletely averaged and results in biexponential relaxation rates (fast and slow components). In biological tissues, the presence of biexponential relaxation rates and the incomplete averaging of the quadripolar interaction results in the creation of multiple quantum coherences. The quadripolar coupling of sodium in cartilage has also been reported to correlate with early degenerative changes.[137,138]

The lower physiological sodium concentration (110 M versus 300 mM), 3.8-fold smaller gyromagnetic ratio in biological tissues, and shorter T2 relaxation time make sodium MRI less attractive in many respects compared with conventional proton MRI. Therefore, one has to compromise image quality to gain sensitivity. The short T1 of sodium (~20 ms) allows for rapid signal averaging, which partially offsets the loss in signal/unit time. Sodium MRI is advantageous in investigating pathology where the change in sodium MR properties of the tissue of interest is more pronounced than the changes in relaxation times and water content. The negatively charged GAG plays an important role in determining tissue integrity by maintaining a fixed charge density (FCD) in cartilage. Positively charged sodium ions are attracted by the FCD. There is a strong correlation between FCD and GAG.[55,139] Previous studies have already shown that sodium MRI has a potential advantage over conventional proton MRI in investigating biochemical markers in cartilage during the early stages of OA.[19,55,140–142]

In general, the transverse relaxation is characterized by a fast or broad resonance component (shorter T2) that contains 60% of the total sodium signal, representing the transitions from +3/2 to +1/2 and from −3/2 to −1/2. The slow or narrow component (longer T2) of the sodium signal represents 40% of the total signal, and the transition from +1/2 to −1/2. The relative magnitude of narrow/broad line widths depends on the strength of the quadripolar interaction. Typical transverse relaxation times in cartilage, for example, are between 1 and 3 ms for the fast component and 8 and 15 ms for the slow component.[141,142] The fast component of T2 may not be visible on conventional MR pulse sequences because of echo time limitations.

To avoid signal loss due to the fast T2 component, sodium MRI requires both innovative 3D ultra-short echo-pulse sequences (3D-UTE) that achieve short echo times as well as high field systems (≥3 T) for adequate SNR. Even at 3 T, the sodium imaging time of the whole knee joint would be ~30 to 45 minutes to achieve adequate SNR. Recent advances in magnet technology, improved gradient performance, multicoil RF technology (parallel receive as well as transmit) may make sodium MRI clinically feasible on high fields systems. Strong evidence indicates that an ultrahigh field 7T-MRI system will further improve sensitivity, specificity, and spatial and temporal resolution. More importantly, the 7T-MRI system would be most suitable to image low gamma nuclei such as sodium (OA) and phosphorus (osteoporosis and skeletal muscle diseases) and may provide disease-specific molecular and functional information on musculoskeletal systems. Although sodium MRI has high specificity and does not require any exogenous contrast agent, it does require special hardware capabilities (multinuclear), specialized RF coils (transmit/receive), and likely 3D ultrashort TE sequences. These challenges currently limit the clinical use of sodium MRI at standard clinical scanners. We have recently implemented the 3D-UTE imaging sequence on 3 T and 7 T, and Fig. 5 shows the representative sodium MRI results.

Magnetization Transfer and Chemical Exchange Saturation Transfer

Balaban and his colleagues[143–145] were the first to demonstrate that the chemical exchange between labile protons of low concentration solutes and bulk water protons provides a sensitivity enhancement scheme known as CEST. After this initial work on small solutes, Zhou et al[146–148] showed that endogenous mobile proteins and peptides at very low concentration in biological tissue could also be detected via the bulk water signal.

In brief, using an amide proton transfer imaging approach, in which the endogenous composite amide resonance at 8.3 ppm (rat brain) is saturated, chemical exchange could be detected indirectly by MRI (tissue pH, protein, and peptide content). The exchange between small and large proton pools in principle would need to include both conventional MT contrast based on the magnetization exchange between cellular solid and semisolid phases and the water protons, as well as the recent approach of CEST imaging, based on chemical exchange between protons of solutes and bulk water.

MT is an extremely common physical phenomenon in MRI. Conventional MT measurements in vivo have been based on the presence of a semisolid macro-molecular phase with a spectral width as large as 10 KHz that is approximately field strength dependent. When saturation is applied at a particular frequency far from the water resonance, this saturation is transferred rapidly between solid-like matrix (rigid collagen) and free bulk water. Therefore, two possible molecular mechanisms are responsible for MT. The first pathway is through-space dipolar coupling from (1) protons of the immobilized macromolecular phase, (2) protons of hydration water on the macromolecular surface, and (3) protons of the unbound bulk water. The second pathway is through the protons of some side groups (e.g., ^{-}NH, $^{-}NH_2$, ^{-}OH, etc.), which mix with water protons via fast chemical exchange.

In MT experiments, RF saturation effects on water are often displayed as a function of saturation frequency offset relative to bulk water (set to 0 ppm by convention). This was originally referred to as an MT spectrum or Z spectrum or, more recently, as a CEST spectrum in which the effect of saturation transfer at a specific irradiation frequency can be identified readily. Conventional MT[149,150] can be detected over a very large frequency range (±100 KHz). This frequency range is determined by the dipolar interaction and chemical shift anisotropy for semisolid macromolecules in tissue. However, CEST is usually detected in a small chemical shift range of less than ± 5 ppm from bulk water. The main difference between MT and CEST are the frequency specificity of the CEST saturation

effect and the approximately symmetrical appearance of conventional MT with respect to the water resonance. However, CEST effects originate from mobile molecules and depend purely on chemical exchange, whereas conventional MT depends on both chemical exchange and cross-relaxation. The CEST contrast also strongly depends on pH and temperature. Furthermore, it has been reported by several investigators[66,151] that only rigid collagen macromolecules, and not PG, are responsible for conventional MT contrast in cartilage.

Interestingly, both PG and collagen macromolecules have exchangeable amide protons (~100 mM) that exchange with bulk water. In addition, each PG unit also has three $^{-}$OH protons (~300 mM) that rapidly exchange with bulk water. Similarly, collagen has exchangeable amine protons ($^{-}NH_2$). Recently, Ling et al[41] extensively studied and identified the potential metabolites in the cartilage via ^{1}H and ^{13}C one- and two-dimensional nuclear magnetic resonance spectroscopy as well as CEST methods. Furthermore feasibility of the CEST method was also demonstrated in model systems, bovine cartilage, and an in vivo human volunteer (Fig. 6) on a 3-T clinical scanner.[42] This CEST method currently is still in the embryonic stage, and more extensive studies and validation are required.

CONCLUSION

MR imaging is a powerful noninvasive technique for the quantitative assessment of musculoskeletal disorders in general and articular cartilage in particular. New quantitative 3D-MRI methods at high field systems (≥3 T) are rapidly emerging and hold promise to detect early biochemical and functional changes in OA. Recent technological developments (high field MR systems, new imaging methods, novel 3D-pulse sequences, parallel RF transmit/receive, etc.) will further enhance not only our ability to characterize the musculoskeletal diseases but also to improve the potential clinical outcomes. New emerging rapid-3D high-resolution biochemical imaging methods at high field systems have great potential for evaluating early signs of OA before morphological changes occur. We believe that in the near future the biochemical imaging methods will play an increasingly important role in the management of OA with disease-modifying therapies. We have emphasized the effects of higher field strength on these contrast mechanisms.

Acknowledgments

This work was supported by research grant R01-AR053133–01A2 from the National Institute of Arthritis and Musculoskeletal and Skin Diseases (NIAMS), National Institutes of Health (NIH).

References

1. Felson DT. Clinical practice. Osteoarthritis of the knee. N Engl J Med. 2006; 354:841–848. [PubMed: 16495396]
2. Felson DT, Niu J, Guermazi A, et al. Correlation of the development of knee pain with enlarging bone marrow lesions on magnetic resonance imaging. Arthritis Rheum. 2007; 56:2986–2992. [PubMed: 17763427]
3. Felson DT, Kim YJ. The futility of current approaches to chondroprotection. Arthritis Rheum. 2007; 56:1378–1383. [PubMed: 17469094]
4. Felson DT. Risk factors for osteoarthritis: understanding joint vulnerability. Clin Orthop Relat Res. 2004:S16–S21. [PubMed: 15480060]
5. Brandt, HJ.; Ma, KD. Osteoarthritis: Diagnosis and Medical/ Surgical Management. Philadelphia, Pa: WB Saunders; 1992.
6. Sharma L, Song J, Felson DT, Cahue S, Shamiyeh E, Dunlop DD. The role of knee alignment in disease progression and functional decline in knee osteoarthritis. JAMA. 2001; 286:188–195. [PubMed: 11448282]

7. Sharma L, Chang A. Overweight: advancing our understanding of its impact on the knee and the hip. Ann Rheum Dis. 2007; 66:141–142. [PubMed: 17242017]
8. Sharma L. Nonpharmacologic management of osteoarthritis. Curr Opin Rheumatol. 2002; 14:603–607. [PubMed: 12192263]
9. Sharma L. Local factors in osteoarthritis. Curr Opin Rheumatol. 2001; 13:441–446. [PubMed: 11604602]
10. Nevitt MC, Sharma L. OMERACT workshop radiography session 1. Osteoarthritis Cartilage. 2006; 14(suppl A):A4–A9. [PubMed: 16753308]
11. Buckland-Wright JC, Ward RJ, Peterfy C, Mojcik CF, Leff RL. Reproducibility of the semiflexed (metatarsophalangeal) radiographic knee position and automated measurements of medial tibiofemoral joint space width in a multicenter clinical trial of knee osteoarthritis. J Rheumatol. 2004; 31:1588–1597. [PubMed: 15290740]
12. Le Graverand MP, Mazzuca S, Lassere M, Guermazi A, Pickering E, Brandt K, et al. Assessment of the radio-anatomic positioning of the osteoarthritic knee in serial radiographs: comparison of three acquisition techniques. Osteoarthritis Cartilage. 2006; 14(suppl A):A37–A43. [PubMed: 16785057]
13. Peterfy C, Kothari M. Imaging osteoarthritis: magnetic resonance imaging versus X-ray. Curr Rheumatol Rep. 2006; 8:16–21. [PubMed: 16515760]
14. Gale DR, Chaisson CE, Totterman SM, Schwartz RK, Gale ME, Felson D. Meniscal subluxation: association with osteoarthritis and joint space narrowing. Osteoarthritis Cartilage. 1999; 7:526–532. [PubMed: 10558850]
15. Hunter DJ, Zhang YQ, Tu X, et al. Change in joint space width: hyaline articular cartilage loss or alteration in meniscus? Arthritis Rheum. 2006; 54:2488–2495. [PubMed: 16868968]
16. Bashir A, Gray ML, Burstein D. Gd-DTPA^{2-} as a measure of cartilage degradation. Magn Reson Med. 1996; 36:665–673. [PubMed: 8916016]
17. Bashir A, Gray ML, Boutin RD, Burstein D. Glycosaminoglycan in articular cartilage: in vivo assessment with delayed Gd(DTPA)$^{2-}$-enhanced MR imaging. Radiology. 1997; 205:551–558. [PubMed: 9356644]
18. Mosher TJ, Dardzinski BJ, Smith MB. Human articular cartilage: influence of aging and early symptomatic degeneration on the spatial variation of T2—preliminary findings at 3 T. Radiology. 2000; 214:259–266. [PubMed: 10644134]
19. Reddy R, Insko EK, Noyszewski EA, Dandora R, Kneeland JB, Leigh JS. Sodium MRI of human articular cartilage in vivo. Magn Reson Med. 1998; 39:697–701. [PubMed: 9581599]
20. Regatte RR, Akella SV, Wheaton AJ, et al. 3D–T1rho-relaxation mapping of articular cartilage: in vivo assessment of early degenerative changes in symptomatic osteoarthritic subjects. Acad Radiol. 2004; 11:741–749. [PubMed: 15217591]
21. Regatte RR, Akella SV, Borthakur A, Kneeland JB, Reddy R. In vivo proton MR three-dimensional T1rho mapping of human articular cartilage: initial experience. Radiology. 2003; 229:269–274. [PubMed: 14519880]
22. Li X, Benjamin Ma C, Link TM, et al. In vivo T(1rho) and T(2) mapping of articular cartilage in osteoarthritis of the knee using 3 T MRI. Osteoarthritis Cartilage. 2007; 15:789–797. [PubMed: 17307365]
23. Li X, Han ET, Busse RF, Majumdar S. In vivo T(1rho) mapping in cartilage using 3D magnetization-prepared angle-modulated partitioned k-space spoiled gradient echo snapshots (3D MAPSS). Magn Reson Med. 2008; 59:298–307. [PubMed: 18228578]
24. Li X, Han ET, Ma CB, Link TM, Newitt DC, Majumdar S. In vivo 3T spiral imaging based multi-slice T(1rho) mapping of knee cartilage in osteoarthritis. Magn Reson Med. 2005; 54:929–936. [PubMed: 16155867]
25. Pakin SK, Cavalcanti C, La Rocca R, Schweitzer ME, Regatte RR. Ultra-high-field MRI of knee joint at 7. 0T: preliminary experience. Acad Radiol. 2006; 13:1135–1142. [PubMed: 16935725]
26. Pakin SK, Xu J, Schweitzer ME, Regatte RR. Rapid 3D–T1rho mapping of the knee joint at 3. 0T with parallel imaging. Magn Reson Med. 2006; 56:563–571. [PubMed: 16894582]
27. Pakin SK, Schweitzer ME, Regatte RR. 3D–T1rho quantitation of patellar cartilage at 3. 0T. J Magn Reson Imaging. 2006; 24:1357–1363. [PubMed: 17058202]

28. Gold GE, Hargreaves BA, Reeder SB, et al. Balanced SSFP imaging of the musculoskeletal system. J Magn Reson Imaging. 2007; 25:270–278. [PubMed: 17260387]
29. Gold GE, Busse RF, Beehler C, et al. Isotropic MRI of the knee with 3D fast spin-echo extended echotrain acquisition (XETA): initial experience. AJR Am J Roentgenol. 2007; 188:1287–1293. [PubMed: 17449772]
30. Gold GE, Reeder SB, Yu H, et al. Articular cartilage of the knee: rapid three-dimensional MR imaging at 3. 0 T with IDEAL balanced steady-state free precession—initial experience. Radiology. 2006; 240:546–551. [PubMed: 16801369]
31. Gold GE, Han E, Stainsby J, Wright G, Brittain J, Beaulieu C. Musculoskeletal MRI at 3. 0 T: relaxation times and image contrast. AJR Am J Roentgenol. 2004; 183:343–351. [PubMed: 15269023]
32. Gold GE. Dynamic and functional imaging of the musculoskeletal system. Semin Musculoskelet Radiol. 2003; 7:245–248. [PubMed: 14735424]
33. Dardzinski BJ, Mosher TJ, Li SZ, VanSlyke MA, Smith MB. Spatial variation of T2 in human articular cartilage. Radiology. 1997; 205:546–550. [PubMed: 9356643]
34. David-Vaudey E, Ghosh S, Ries M, Majumdar S. T2 relaxation time measurements in osteoarthritis. Magn Reson Imaging. 2004; 22:673–682. [PubMed: 15172061]
35. Eckstein F, Mosher T, Hunter D. Imaging of knee osteoarthritis: data beyond the beauty. Curr Opin Rheumatol. 2007; 19:435–443. [PubMed: 17762608]
36. Eckstein F, Burstein D, Link TM. Quantitative MRI of cartilage and bone: degenerative changes in osteoarthritis. NMR Biomed. 2006; 19:822–854. [PubMed: 17075958]
37. Eckstein F, Ateshian G, Burgkart R, et al. Proposal for a nomenclature for magnetic resonance imaging based measures of articular cartilage in osteoarthritis. Osteoarthritis Cartilage. 2006; 14:974–983. [PubMed: 16730462]
38. Eckstein F, Hudelmaier M, Wirth W, et al. Double echo steady state magnetic resonance imaging of knee articular cartilage at 3 Tesla: a pilot study for the Osteoarthritis Initiative. Ann Rheum Dis. 2006; 65:433–441. [PubMed: 16126797]
39. Eckstein F, Hudelmaier M, Putz R. The effects of exercise on human articular cartilage. J Anat. 2006; 208:491–512. [PubMed: 16637874]
40. Eckstein F, Kunz M, Schutzer M, et al. Two year longitudinal change and test-retest-precision of knee cartilage morphology in a pilot study for the osteoarthritis initiative. Osteoarthritis Cartilage. 2007; 15:1326–1332. [PubMed: 17560813]
41. Ling W, Regatte RR, Schweitzer ME, Jerschow A. Characterization of bovine patellar cartilage by NMR. NMR Biomed. 2008; 21(3):289–295. [PubMed: 17659534]
42. Ling W, Regatte RR, Navon G, Jerschow A. Assessment of glycosaminoglycan concentration in vivo by chemical exchange-dependent saturation transfer (gagCEST). Proc Natl Acad Sci U S A. 2008; 105(7):2266–2270. [PubMed: 18268341]
43. Link TM, Sell CA, Masi JN, et al. 3.0 vs 1. 5T MRI in the detection of focal cartilage pathology—ROC analysis in an experimental model. Osteoarthritis Cartilage. 2006; 14(1):63–70. [PubMed: 16188466]
44. Link TM, Stahl R, Woertler K. Cartilage imaging: motivation, techniques, current and future significance. Eur Radiol. 2007; 17:1135–1146. [PubMed: 17093967]
45. Wheaton AJ, Borthakur A, Kneeland JB, Regatte RR, Akella SV, Reddy R. In vivo quantification of T1rho using a multislice spin-lock pulse sequence. Magn Reson Med. 2004; 52:1453–1458. [PubMed: 15562469]
46. Wheaton AJ, Borthakur A, Charagundla SR, Reddy R. Pulse sequence for multislice T1rho-weighted MRI. Magn Reson Med. 2004; 51:362–369. [PubMed: 14755662]
47. Wheaton AJ, Borthakur A, Dodge GR, Kneeland JB, Schumacher HR, Reddy R. Sodium magnetic resonance imaging of proteoglycan depletion in an in vivo model of osteoarthritis. Acad Radiol. 2004; 11:21–28. [PubMed: 14746398]
48. Wheaton AJ, Borthakur A, Shapiro EM, et al. Proteogly-can loss in human knee cartilage: quantitation with sodium MR imaging—feasibility study. Radiology. 2004; 231:900–905. [PubMed: 15163825]

49. Witschey WR II, Borthakur A, Elliott MA, et al. Artifacts in T1 rho-weighted imaging: compensation for B(1) and B(0) field imperfections. J Magn Reson. 2007; 186:75–85. [PubMed: 17291799]
50. Witschey WR, Borthakur A, Elliott MA, et al. Compensation for spin-lock artifacts using an off-resonance rotary echo in T1rho off-weighted imaging. Magn Reson Med. 2007; 57:2–7. [PubMed: 17191245]
51. McKenzie CA, Williams A, Prasad PV, Burstein D. Three-dimensional delayed gadolinium-enhanced MRI of cartilage (dGEMRIC) at 1.5T and 3. 0T. J Magn Reson Imaging. 2006; 24:928–933. [PubMed: 16941612]
52. Wang L, Schweitzer ME, Padua A, Regatte RR. Rapid 3D-T(1) mapping of cartilage with variable flip angle and parallel imaging at 3. 0T. J Magn Reson Imaging. 2008; 27:154–161. [PubMed: 18050327]
53. Reeder SB, McKenzie CA, Pineda AR, et al. Water-fat separation with IDEAL gradient-echo imaging. J Magn Reson Imaging. 2007; 25:644–652. [PubMed: 17326087]
54. Reeder SB, Pelc NJ, Alley MT, Gold GE. Rapid MR imaging of articular cartilage with steady-state free precession and multipoint fat-water separation. AJR Am J Roentgenol. 2003; 180:357–362. [PubMed: 12540434]
55. Shapiro EM, Borthakur A, Gougoutas A, Reddy R. 23Na MRI accurately measures fixed charge density in articular cartilage. Magn Reson Med. 2002; 47:284–291. [PubMed: 11810671]
56. Mlynarik V, Szomolanyi P, Toffanin R, Vittur F, Trattnig S. Transverse relaxation mechanisms in articular cartilage. J Magn Reson. 2004; 169:300–307. [PubMed: 15261626]
57. Mlynarik V, Sulzbacher I, Bittsansky M, Fuiko R, Trattnig S. Investigation of apparent diffusion constant as an indicator of early degenerative disease in articular cartilage. J Magn Reson Imaging. 2003; 17:440–444. [PubMed: 12655583]
58. Mlynarik V, Degrassi A, Toffanin R, Vittur F, Cova M, Pozzi-Mucelli RS. Investigation of laminar appearance of articular cartilage by means of magnetic resonance microscopy. Magn Reson Imaging. 1996; 14:435–442. [PubMed: 8782182]
59. Xia Y, Farquhar T, Burton-Wurster N, Lust G. Origin of cartilage laminae in MRI. J Magn Reson Imaging. 1997; 7:887–894. [PubMed: 9307916]
60. Xia Y. Relaxation anisotropy in cartilage by NMR microscopy (μMRI) at 14-μm resolution. Magn Reson Med. 1998; 39:941–949. [PubMed: 9621918]
61. Xia Y, Moody JB, Alhadlaq H. Orientational dependence of T2 relaxation in articular cartilage: A microscopic MRI (microMRI) study. Magn Reson Med. 2002; 48:460–469. [PubMed: 12210910]
62. Xia Y, Moody JB, Alhadlaq H, Hu J. Imaging the physical and morphological properties of a multi-zone young articular cartilage at microscopic resolution. J Magn Reson Imaging. 2003; 17:365–374. [PubMed: 12594728]
63. Bloch F, Hansen WW, Packard M. Nuclear induction. Phys Rev. 1946; 69:127.
64. Blumenkrantz G, Li X, Han ET, et al. A feasibility study of in vivo T1rho imaging of the intervertebral disc. Magn Reson Imaging. 2006; 24:1001–1007. [PubMed: 16997069]
65. Burstein D. MRI for development of disease-modifying osteoarthritis drugs. NMR Biomed. 2006; 19:669–680. [PubMed: 16986116]
66. Burstein D, Bashir A, Gray ML. MRI techniques in early stages of cartilage disease. Invest Radiol. 2000; 35:622–638. [PubMed: 11041156]
67. Kimelman T, Vu A, Storey P, McKenzie C, Burstein D, Prasad P. Three-dimensional T1 mapping for dGEMRIC at 3. 0 T using the Look Locker method. Invest Radiol. 2006; 41:198–203. [PubMed: 16428993]
68. Roos EM, Dahlberg L. Positive effects of moderate exercise on glycosaminoglycan content in knee cartilage: a four-month, randomized, controlled trial in patients at risk of osteoarthritis. Arthritis Rheum. 2005; 52:3507–3514. [PubMed: 16258919]
69. Williams A, Mikulis B, Krishnan N, Gray M, McKenzie C, Burstein D. Suitability of T(1Gd) as the dGEMRIC index at 1.5T and 3. 0T. Magn Reson Med. 2007; 58:830–834. [PubMed: 17899599]
70. Williams A, Sharma L, McKenzie CA, Prasad PV, Burstein D. Delayed gadolinium-enhanced magnetic resonance imaging of cartilage in knee osteoarthritis: findings at different radiographic

stages of disease and relationship to malalignment. Arthritis Rheum. 2005; 52:3528–3535. [PubMed: 16255024]

71. Lammentausta E, Silvast TS, Narvainen J, Jurvelin JS, Nieminen MT, Grohn OHT. T2, Carr-Purcell T2 and T1rho of fat and water as surrogate markers of trabecular bone structure. Phys Med Biol. 2008; 53:543–555. [PubMed: 18199901]
72. Lammentausta E, Kiviranta P, Toyras J, et al. Quantitative MRI of parallel changes of articular cartilage and underlying trabecular bone in degeneration. Osteoarthritis Cartilage. 2007; 15:1149–1157. [PubMed: 17502160]
73. Lammentausta E, Kiviranta P, Nissi MJ, et al. T2 relaxation time and delayed gadolinium-enhanced MRI of cartilage (dGEMRIC) of human patellar cartilage at 1.5 T and 9. 4 T: relationships with tissue mechanical properties. J Orthop Res. 2006; 24:366–374. [PubMed: 16479569]
74. Recht MP, Resnick D. MR imaging of articular cartilage: current status and future directions. AJR Am J Roentgenol. 1994; 163:283–290. [PubMed: 8037016]
75. Recht MP, Piraino DW, Paletta GA, Schils JP, Belhobek GH. Accuracy of fat-suppressed three-dimensional spoiled gradient-echo FLASH MR imaging in the detection of patellofemoral articular cartilage abnormalities. Radiology. 1996; 198:209–212. [PubMed: 8539380]
76. Recht MP, Resnick D. Magnetic resonance imaging of articular cartilage: an overview [Review] [69 refs]. Top Magn Reson Imaging. 1998; 9:328–336. [PubMed: 9894736]
77. Huber M, Trattnig S, Lintner F. Anatomy, biochemistry, and physiology of articular cartilage. Invest Radiol. 2000; 35:573–580. [PubMed: 11041151]
78. Huster D, Schiller J, Arnold K. Dynamics of collagen in articular cartilage studied by solid-state NMR methods. Methods Mol Med. 2004; 101:303–318. [PubMed: 15299222]
79. Hodgeson, RJ.; Carpenter, TA.; Hall, LD. Articular Cartilage and Osteoarthritis. New York: Raven; 1991.
80. Venn M, Maroudas A. Chemical composition and swelling of normal and osteoarthrotic femoral head cartilage. I. Chemical composition. Ann Rheum Dis. 1977; 36:121–129. [PubMed: 856064]
81. Carney SL, Muir H. The structure and function of cartilage proteoglycans. Physiol Rev. 1988; 68:858–910. [PubMed: 3293094]
82. Mankin, HJ.; Brandt, KD. Biochemistry and metabolism of articular cartilage in osteoarthritis. In: Moskowitz, RW.; Howell, DS.; Goldberg, VM.; Mankin, HJ., editors. Osteoarthritis: Diagnosis and Medical/Surgical Management. Philadelphia, Pa: WB Saunders; 1992. p. 109-154.
83. Roughley PJ, Lee ER. Cartilage proteoglycans: structure and potential functions. Microsc Res Tech. 1994; 28:385–397. [PubMed: 7919526]
84. Moskowitz, RW.; Howell, DS.; Goldberg, VM.; Mankin, HJ. Osteoarthritis: Diagnosis and Medical/Surgical Management. Philadelphia, Pa: WB Saunders; 1992. p. 761
85. Xia Y, Farquhar T, Burton-Wurster N, Ray E, Jelinski LW. Diffusion and relaxation mapping of cartilage-bone plugs and excised disks using microscopic magnetic resonance imaging. Magn Reson Med. 1994; 31:273–282. [PubMed: 8057798]
86. Mosher TJ. Musculoskeletal imaging at 3T: current techniques and future applications. Magn Reson Imaging Clin N Am. 2006; 14:63–76. [PubMed: 16530635]
87. Mosher TJ, Smith HE, Collins C, et al. Change in knee cartilage T2 at MR imaging after running: a feasibility study. Radiology. 2005; 234:245–249. [PubMed: 15550376]
88. Mosher TJ, Dardzinski BJ. Cartilage MRI T2 relaxation time mapping: overview and applications. Semin Musculoskelet Radiol. 2004; 8:355–368. [PubMed: 15643574]
89. Eckstein F, Gavazzeni A, Sittek H, et al. Determination of knee joint cartilage thickness using three- dimensional magnetic resonance chondro-crassometry (3D MR-CCM). Magn Reson Med. 1996; 36:256–265. [PubMed: 8843380]
90. Eckstein F, Sittek H, Gavazzeni A, et al. Magnetic resonance chondro-crassometry (MR CCM): a method for accurate determination of articular cartilage thickness. Magn Reson Med. 1996; 35:89–96. [PubMed: 8771026]
91. Eckstein F, Schnier M, Haubner M, et al. Accuracy of cartilage volume and thickness measurements with magnetic resonance imaging. Clin Orthop Relat Res. 1998:137–148. [PubMed: 9678042]

92. Eckstein F, Adam C, Sittek H, et al. Non-invasive determination of cartilage thickness throughout joint surfaces using magnetic resonance imaging. J Biomech. 1997; 30:285–289. [PubMed: 9119830]
93. Eckstein F, Englmeier KH. Quantitative image analysis: software systems in drug development trials. Drug Discov Today. 2003; 8:922–923. [PubMed: 14554153]
94. Eckstein F, Buck RJ, Wyman BT, et al. Quantitative imaging of cartilage morphology at 3. 0 Tesla in the presence of gadopentetate dimeglumine (Gd-DTPA). Magn Reson Med. 2007; 58:402–406. [PubMed: 17654593]
95. Eckstein F, Kunz M, Hudelmaier M, et al. Impact of coil design on the contrast-to-noise ratio, precision, and consistency of quantitative cartilage morphometry at 3 Tesla: a pilot study for the Osteoarthritis Initiative. Magn Reson Med. 2007; 57:448–454. [PubMed: 17260363]
96. Waterton JC, Solloway S, Foster JE, et al. Diurnal variation in the femoral articular cartilage of the knee in young adult humans. Magn Reson Med. 2000; 43:126–132. [PubMed: 10642739]
97. Otterness IG, Eckstein F. Women have thinner cartilage and smaller joint surfaces than men after adjustment for body height and weight. Osteoarthritis Cartilage. 2007; 15:666–672. [PubMed: 17321168]
98. Wang Y, Ding C, Wluka AE, et al. Factors affecting progression of knee cartilage defects in normal subjects over 2 years. Rheumatology. 2006; 45:79–84. [PubMed: 16188947]
99. Borthakur A, Mellon E, Niyogi S, Witschey W, Kneeland JB, Reddy R. Sodium and T1rho MRI for molecular and diagnostic imaging of articular cartilage. NMR Biomed. 2006; 19:781–821. [PubMed: 17075961]
100. Gold GE, McCauley TR, Gray ML, Disler DG. What's new in cartilage? Radiographics. 2003; 23:1227–1242. [PubMed: 14518449]
101. Gold GE, Burstein D, Dardzinski B, Lang P, Boada F, Mosher T. MRI of articular cartilage in OA: novel pulse sequences and compositional/functional markers. Osteoarthritis Cartilage. 2006; 14(suppl A):A76–A86. [PubMed: 16716605]
102. Tiderius C, Hori M, Williams A, et al. dGEMRIC as a function of BMI. Osteoarthritis Cartilage. 2006; 14:1091–1097. [PubMed: 16782361]
103. Bashir A, Gray ML, Hartke J, Burstein D. Nondestructive imaging of human cartilage glycosaminoglycan concentration by MRI. Magn Reson Med. 1999; 41:857–865. [PubMed: 10332865]
104. Burstein D, Velyvis J, Scott KT, et al. Protocol issues for delayed Gd(DTPA)2-enhanced MRI (dGEMRIC) for clinical evaluation of articular cartilage. Magn Reson Med. 2001; 45:36–41. [PubMed: 11146483]
105. Todd DJ, Kagan A, Chibnik LB, Kay J. Cutaneous changes of nephrogenic systemic fibrosis: predictor of early mortality and association with gadolinium exposure [see comment]. Arthritis Rheum. 2007; 56:3433–3441. [PubMed: 17907148]
106. Ersoy H, Rybicki FJ. Biochemical safety profiles of gadolinium-based extracellular contrast agents and nephrogenic systemic fibrosis. J Magn Reson Imaging. 2007; 26:1190–1197. [PubMed: 17969161]
107. Shapiro EM, Borthakur A, Kaufman JH, Leigh JS, Reddy R. Water distribution patterns inside bovine articular cartilage as visualized by 1H magnetic resonance imaging. Osteoarthritis Cartilage. 2001; 9:533–538. [PubMed: 11520167]
108. Lusse S, Claassen H, Gehrke T, et al. Evaluation of water content by spatially resolved transverse relaxation times of human articular cartilage. Magn Reson Imaging. 2000; 18:423–430. [PubMed: 10788720]
109. Lehner KB, Rechl HP, Gmeinwieser JK, Heuck AF, Lukas HP, Kohl HP. Structure, function, and degeneration of bovine hyaline cartilage: assessment with MR imaging in vitro. Radiology. 1989; 170:495–499. [PubMed: 2911674]
110. Nieminen MT, Rieppo J, Toyras J, et al. T2 relaxation reveals spatial collagen architecture in articular cartilage: a comparative quantitative MRI and polarized light microscopic study. Magn Reson Med. 2001; 46:487–493. [PubMed: 11550240]

111. Nieminen MT, Toyras J, Laasanen MS, Silvennoinen J, Helminen HJ, Jurvelin JS. Prediction of biomechanical properties of articular cartilage with quantitative magnetic resonance imaging. J Biomech. 2004; 37:321–328. [PubMed: 14757451]
112. Nieminen MT, Toyras J, Rieppo J, et al. Quantitative MR microscopy of enzymatically degraded articular cartilage. Magn Reson Med. 2000; 43:676–681. [PubMed: 10800032]
113. Goodwin DW, Zhu H, Dunn JF. In vitro MR imaging of hyaline cartilage: correlation with scanning electron microscopy. AJR Am J Roentgenol. 2000; 174:405–409. [PubMed: 10658715]
114. Dunn TC, Lu Y, Jin H, Ries MD, Majumdar S. T2 relaxation time of cartilage at MR imaging: comparison with severity of knee osteoarthritis. Radiology. 2004; 232:592–598. [PubMed: 15215540]
115. Glaser C, Horng A, Mendlik T, et al. T2 relaxation time in patellar cartilage—global and regional reproducibility at 1. 5 Tesla and 3 Tesla. Rofo. 2007; 179:146–152. [PubMed: 17262244]
116. Glaser C, Mendlik T, Dinges J, et al. Global and regional reproducibility of T2 relaxation time measurements in human patellar cartilage. Magn Reson Med. 2006; 56:527–534. [PubMed: 16894587]
117. Mosher TJ, Liu Y, Yang QX, et al. Age dependency of cartilage magnetic resonance imaging T2 relaxation times in asymptomatic women. Arthritis Rheum. 2004; 50:2820–2828. [PubMed: 15457450]
118. Gold GE, Hargreaves BA, Stevens KJ, Beaulieu CF. Advanced magnetic resonance imaging of articular cartilage. Orthop Clin North Am. 2006; 37:331–347vi. [PubMed: 16846765]
119. Nieminen MT, Menezes NM, Williams A, Burstein D. T2 of articular cartilage in the presence of Gd-DTPA2. Magn Reson Med. 2004; 51:1147–1152. [PubMed: 15170834]
120. Regatte RR, Akella SV, Borthakur A, Kneeland JB, Reddy R. Proteoglycan depletion-induced changes in transverse relaxation maps of cartilage: comparison of T2 and T1rho. Acad Radiol. 2002; 9:1388–1394. [PubMed: 12553350]
121. Filidoro L, Dietrich O, Weber J, et al. High-resolution diffusion tensor imaging of human patellar cartilage: feasibility and preliminary findings. Magn Reson Med. 2005; 53:993–998. [PubMed: 15844163]
122. Deng X, Farley M, Nieminen MT, Gray M, Burstein D. Diffusion tensor imaging of native and degenerated human articular cartilage. Magn Reson Imaging. 2007; 25:168–171. [PubMed: 17275610]
123. Miller KL, Hargreaves BA, Gold GE, Pauly JM. Steady-state diffusion-weighted imaging of in vivo knee cartilage. Magn Reson Med. 2004; 51:394–398. [PubMed: 14755666]
124. Glaser C. New techniques for cartilage imaging: T2 relaxation time and diffusion-weighted MR imaging. Radiol Clin North Am. 2005; 43:641–653. [PubMed: 15893528]
125. Redfield AG. Nuclear magnetic resonance saturation and rotary saturation in solids. Phys Rev. 1955; 98:1787.
126. Santyr GE, Henkelman RM, Bronskill MJ. Spin locking for magnetic resonance imaging with application to human breast. Magn Reson Med. 1989; 12:25–37. [PubMed: 2607958]
127. Santyr GE, Fairbanks EJ, Kelcz F, Sorenson JA. Off-resonance spin locking for MR imaging. Magn Reson Med. 1994; 32:43–51. [PubMed: 8084236]
128. Akella SV, Regatte RR, Gougoutas AJ, Borthakur A, Shapiro EM, Kneeland JB, et al. Proteoglycan-induced changes in T1rho-relaxation of articular cartilage at 4T. 2001; 46(3):419–423.
129. Regatte RR, Akella SV, Lonner JH, Kneeland JB, Reddy R. T1rho relaxation mapping in human osteoarthritis (OA) cartilage: comparison of T1rho with T2. J Magn Reson Imaging. 2006; 23:547–553. [PubMed: 16523468]
130. Hilal SK, Maudsley AA, Ra JB, et al. In vivo NMR imaging of sodium-23 in the human head. J Comput Assist Tomogr. 1985; 9:1–7. [PubMed: 3968256]
131. Maudsley AA, Hilal SK. Biological aspects of sodium-23 imaging. Br Med Bull. 1984; 40:165–166. [PubMed: 6744003]
132. Garner WH, Hilal SK, Lee SW, Spector A. Sodium-23 magnetic resonance imaging of the eye and lens. Proc Natl Acad Sci U S A. 1986; 83:1901–1905. [PubMed: 3006076]

133. Ra JB, Hilal SK, Oh CH, Mun IK. In vivo magnetic resonance imaging of sodium in the human body. Magn Reson Med. 1988; 7:11–22. [PubMed: 3386516]
134. Springer, CS. Biological systems: spin-3/2 nuclei. In: Grant, DM.; Harris, RK., editors. Encyclopedia of Nuclear Magnetic Resonance. New York: John Wiley; 1996. p. 940-951.
135. Reddy R, Li SC, Noyszewski EA, Kneeland JB, Leigh JS. In vivo sodium multiple quantum spectroscopy of human articular cartilage. Magn Reson Med. 1997; 38:207–214. [PubMed: 9256099]
136. Reddy R, Shinnar M, Wang Z, Leigh JS. Multiple-quantum filters of spin-3/2 with pulses of arbitrary flip angle. J Magn Reson B. 1994; 104:148–152. [PubMed: 8049867]
137. Ling W, Regatte RR, Schweitzer ME, Jerschow A. Behavior of ordered sodium in enzymatically depleted cartilage tissue. Magn Reson Med. 2006; 56:1151–1155. [PubMed: 17029232]
138. Navon G, Werrmann JG, Maron R, Cohen SM. 31P NMR and triple quantum filtered 23Na NMR studies of the effects of inhibition of Na +/H +exchange on intracellular sodium and pH in working and ischemic hearts. Magn Reson Med. 1994; 32:556–564. [PubMed: 7808256]
139. Wheaton AJ, Casey FL, Gougoutas AJ, et al. Correlation of T1rho with fixed charge density in cartilage. J Magn Reson Imaging. 2004; 20:519–525. [PubMed: 15332262]
140. Shapiro EM, Borthakur A, Dandora R, Kriss A, Leigh JS, Reddy R. Sodium visibility and quantitation in intact bovine articular cartilage using high field ^{23}Na MRI and MRS. J Magn Reson. 2000; 142:24–31. [PubMed: 10617432]
141. Borthakur A, Mellon E, Niyogi S, Witschey W, Kneeland JB, Reddy R. Sodium and T1rho MRI for molecular and diagnostic imaging of articular cartilage. NMR Biomed. 2006; 19:781–821. [PubMed: 17075961]
142. Borthakur A, Shapiro EM, Beers J, Kudchodkar S, Kneeland JB, Reddy R. Sensitivity of MRI to proteoglycan depletion in cartilage: comparison of sodium and proton MRI. Osteoarthritis Cartilage. 2000; 8:288–293. [PubMed: 10903883]
143. Guivel-Scharen V, Sinnwell T, Wolff SD, Balaban RS. Detection of proton chemical exchange between metabolites and water in biological tissues. J Magn Reson. 1998; 133:36–45. [PubMed: 9654466]
144. Ward KM, Aletras AH, Balaban RS. A new class of contrast agents for MRI based on proton chemical exchange dependent saturation transfer (CEST). J Magn Reson. 2000; 143:79–87. [PubMed: 10698648]
145. Ward KM, Balaban RS. Determination of pH using water protons and chemical exchange dependent saturation transfer (CEST). Magn Reson Med. 2000; 44:799–802. [PubMed: 11064415]
146. Zhou J, Lal B, Wilson DA, Laterra J, van Zijl PC. Amide proton transfer (APT) contrast for imaging of brain tumors. Magn Reson Med. 2003; 50:1120–1126. [PubMed: 14648559]
147. Zhou J, Wilson DA, Sun PZ, Klaus JA, Van Zijl PC. Quantitative description of proton exchange processes between water and endogenous and exogenous agents for WEX, CEST, and APT experiments. Magn Reson Med. 2004; 51:945–952. [PubMed: 15122676]
148. Zhou J, Payen JF, Wilson DA, Traystman RJ, van Zijl PC. Using the amide proton signals of intracellular proteins and peptides to detect pH effects in MRI. Nat Med. 2003; 9:1085–1090. [PubMed: 12872167]
149. Henkelman RM, Stanisz GJ, Graham SJ. Magnetization transfer in MRI: a review. NMR Biomed. 2001; 14:57–64. [PubMed: 11320533]
150. Henkelman RM, Huang X, Xiang QS, Stanisz GJ, Swanson SD, Bronskill MJ. Quantitative interpretation of magnetization transfer. Magn Reson Med. 1993; 29:759–766. [PubMed: 8350718]
151. Wolff SD, Balaban RS. Magnetization transfer contrast (MTC) and tissue water proton relaxation in vivo. Magn Reson Med. 1989; 10:135–144. [PubMed: 2547135]

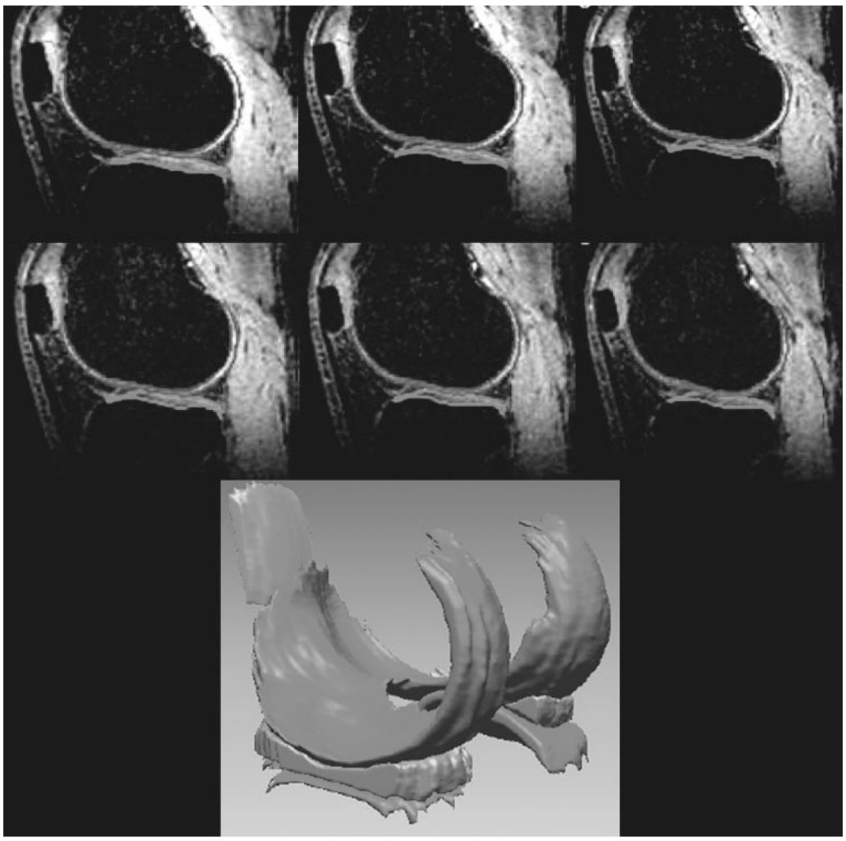

Figure 1.
Representative high-resolution (three-dimensional fast low-angle shot) sagittal knee images with fat suppression were acquired on a healthy volunteer at 7 T for better visualization of cartilage and surrounding structures. Three-dimensional cartilage and menisci volume were reconstructed from corresponding segmented regions; 160 slices were acquired in ~13 minutes with 500 μm × 500 μm × 500 μm isotropic resolution. (From Regatte et al, New York University, Department of Radiology.)

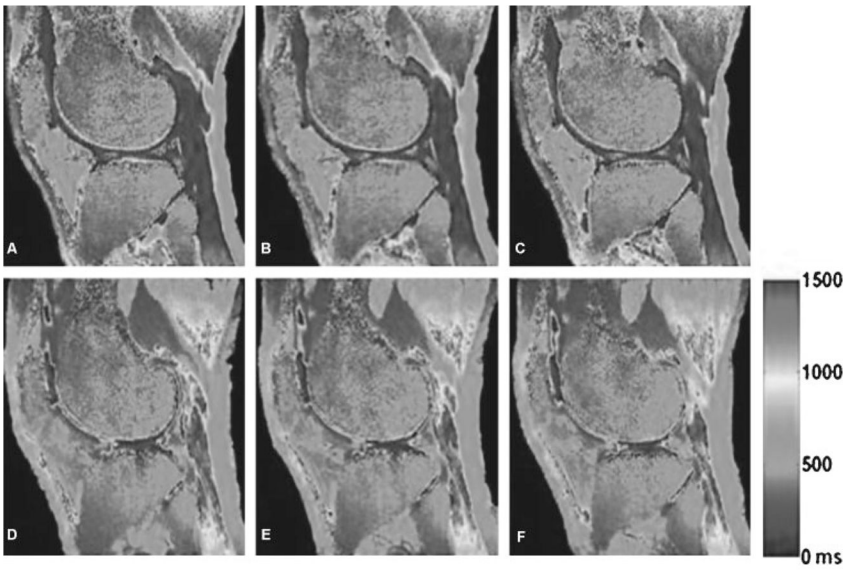

Figure 2.

Representative three-dimensional (3D)-T1 maps of human cartilage acquired using variable flip angles and parallel imaging before and after contrast agent injection in which the T1 values decrease sharply after contrast agent injection. It can be seen that the T1 values of the human cartilage after contrast agent injection are much lower than those of the human cartilage before contrast agent injection. Rapid 3D T1 mapping of the whole knee joint (with 0.7-mm^3 isotropic resolution) was acquired under ~5 minutes at 3.0 T. (From Wang et al, New York University, Department of Radiology.)

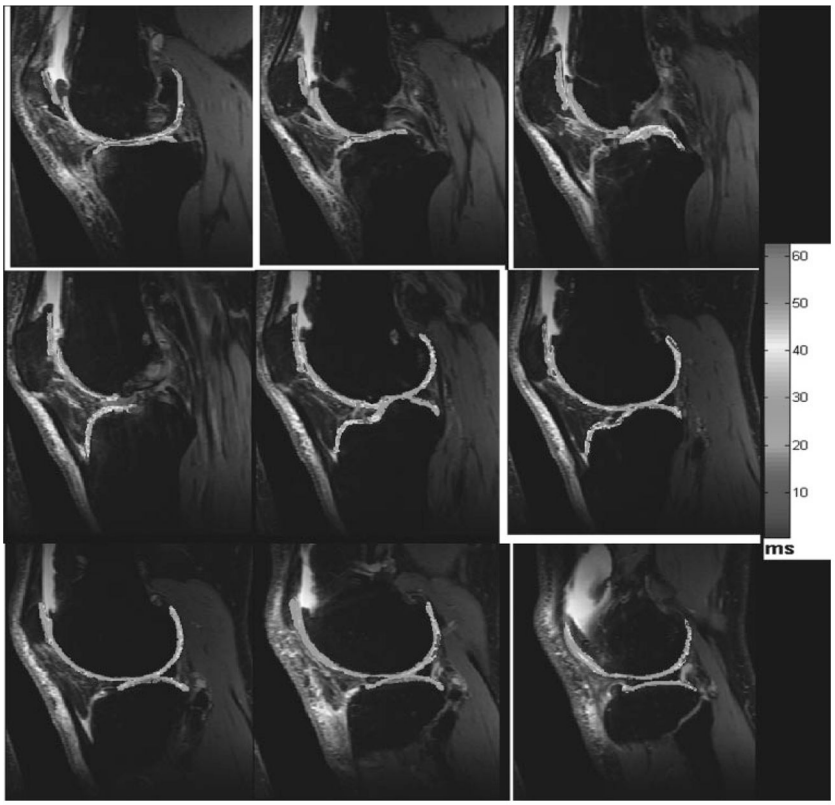

Figure 3.

Series of representative two-dimensional-sagittal T2 maps computed from a patient with osteoarthritis. Two-dimensional-sagittal T2-weighted imaging parameters at 3 T are TR/TE, 4000/16.5, 33, 49.5, 66, 82.5; field of view, 15 cm × 15 cm; matrix, 128 × 256; bandwidth, 130 Hz; slice thickness, 1.5 mm; slice gap, 20%. The color bar scale represents the T2 values in milliseconds (color not shown). (From Wang et al, New York University, Department of Radiology.)

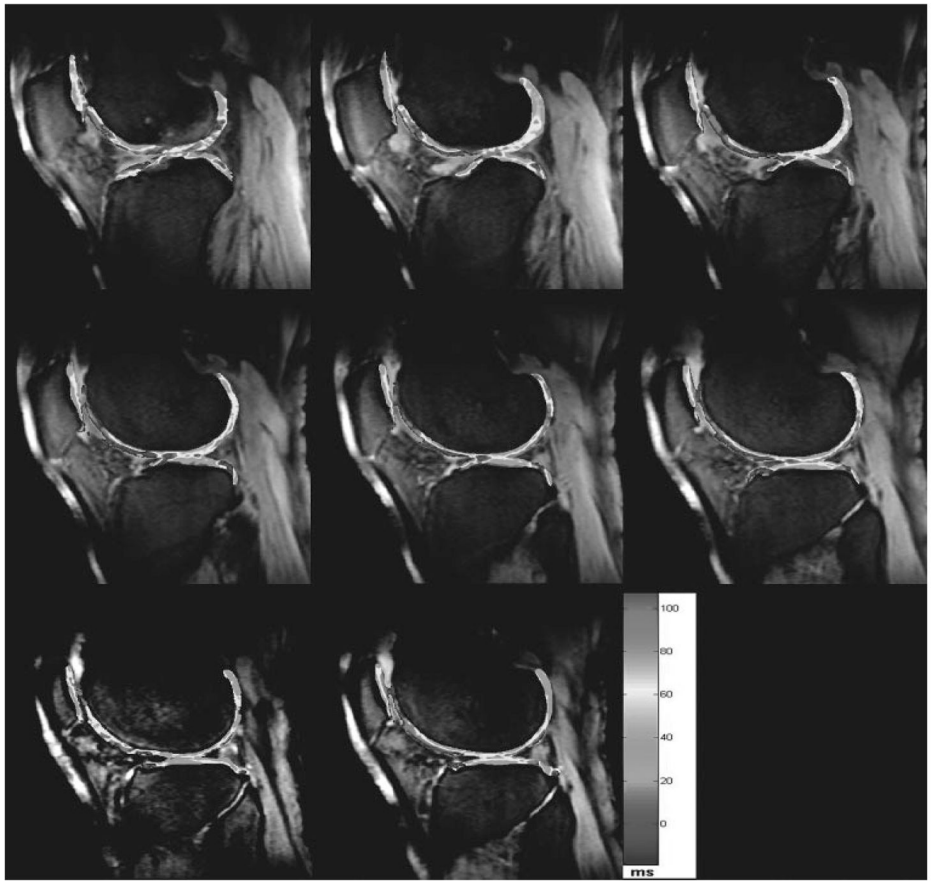

Figure 4.
Representative three-dimensional-$T1_\rho$ maps obtained from a 60-year-old patient with osteoarthritis with parallel imaging (generalized autocalibrating partially parallel acquisitions acceleration factor acceleration factor, 2) and 3D-$T1_\rho$-weighted imaging was performed at 3 T using $T1_\rho$ preparation pulse cluster and 3D-fast low-angle shot as a readout: TR/TE, 175/2.04; spin-lock frequency, 300 Hz; number of slices, 20; time of spin lock, 2/10/20/30 ms; slice thickness, 3 mm; matrix, 256 × 128; field of view, 15 cm; flip angle, 25 degrees; bandwidth, 260 Hz. The color bar scale represents the $T1_\rho$ values in milliseconds (color not shown). (From Regatte et al, New York University, Department of Radiology.)

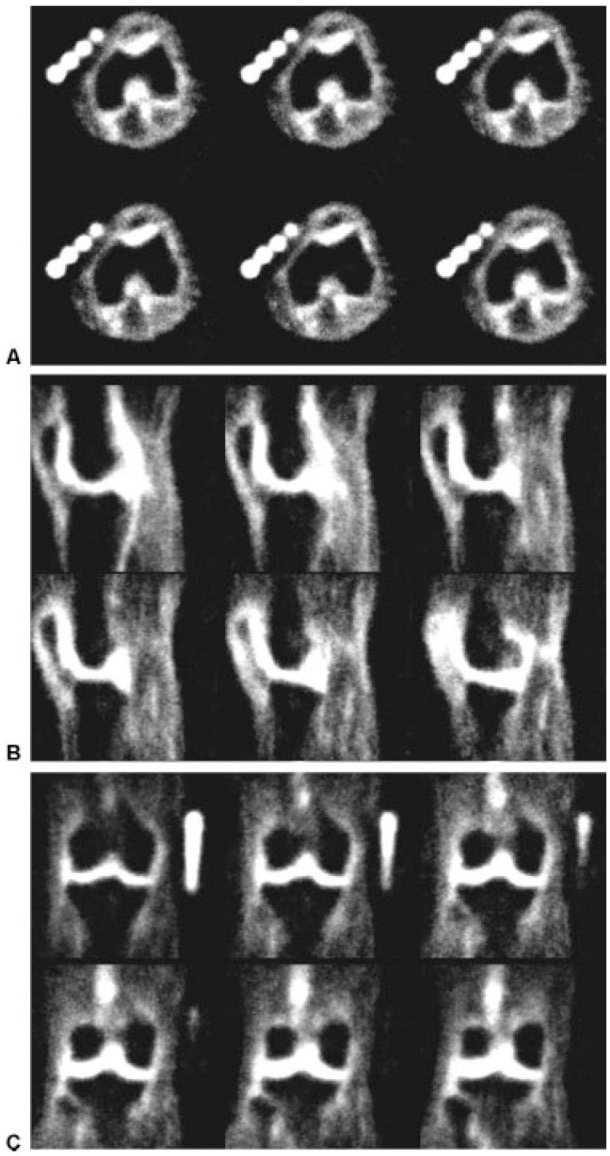

Figure 5.
Rapid high-resolution ^{23}Na–three-dimensional-radial imaging of the knee of a healthy volunteer acquired at 7 T in <14 minutes. Representative slices from all three planes, (A) axial, (B) sagittal, and (C) coronal, are shown. To maximize the detection of a short T2 component, a non-selective 90-degree radiofrequency pulse of 200 μsec was used with a delay of 60 μsec to allow transmit-receive switching delays. The imaging parameters are TR/TE, 80/0.160; averages, 10; slices, 256; spatial resolution, 1.5 mm × 1.5 mm × 1.5 mm; bandwidth, 130 Hz/pixel; radial projections, 1024. (From Regatte et al, New York University, Department of Radiology.)

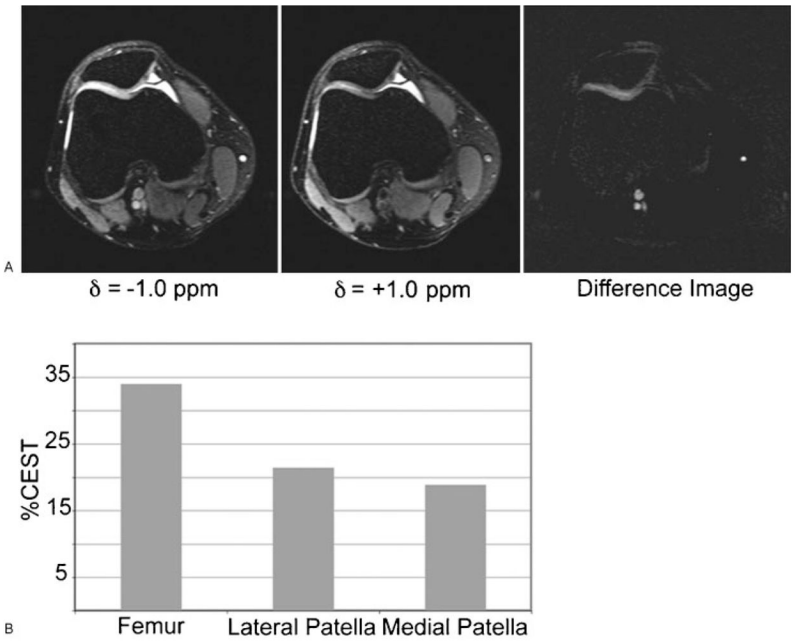

Figure 6.

(A) In vivo images from the human patellofemoral joint of a 27-year-old man with anterior knee pain. CEST (chemical exchange dependent saturation transfer) imaging was performed with irradiation at d =−1.0 ppm, d =+1.0 ppm, and the difference image. (B) The extracted CEST contrast from the femur, the lateral, and the medial sides of the patellofemoral joint. The total duration of the presaturation pulse sequence was 320ms at an average rf power of 42Hz. (From Ling et al, New York University, Department of Chemistry and Radiology.)